PAST KNOWLEDGE PEOPLE

ISSN: 2834-4928

Research Article

Journal of Electrical Electronics Engineering

Dynamical Stability of the LHS 1903 Exoplanetary System: Constraining the Orbital Parameter Space of Planet e and a Putative Fifth Body

Kalash Garg[1*], Tanishq Limbasiya[1] and Ravindran Swamy[2]

[1]*Ekayanaa School, India*

[2]*Senior Physics Faculty, Allen Career Institute, India*

[*]**Corresponding Author**
Kalash Garg, Ekayanaa School, India.

Submitted: 2026, Apr 28; **Accepted**: 2026, May 18; **Published**: 2026, May 28

Citation: Garg, K., Limbasiya, T., Swamy, R. (2026). Dynamical Stability of the LHS 1903 Exoplanetary System: Constraining the Orbital Parameter Space of Planet e and a Putative Fifth Body. *J Electrical Electron Eng, 5*(3), 01-10.

Abstract

We present a comprehensive N-body dynamical stability analysis of the LHS 1903 exoplanetary system, a compact four-planet system orbiting a 0.538$M_\odot$ M-dwarf star recently confirmed by [1]. Using the rebound N-body integration package with the waist simplistic integrator and a timestep of dt = 0.0003 yr, we construct high resolution 50 × 50 survival time maps across 80,000 years — equivalent to approximately 10^6 orbital periods of the outermost confirmed planet — for key orbital parameter combinations centered on the dynamically interesting planet e [2,3]. The nominal system is robustly stable: at the observed mass of planet e ($m_e = 5.79M_\oplus$), the stability boundary lies at $e_d \approx 0.296$, giving a stability margin of $\Delta e_d \approx 0.184$. A companion grid varying the masses of planets d and e independently at nominal eccentricities produces complete stability across all 400 simulations, confirming eccentricity as the dominant driver of instability rather than mass. Analysis of all five resonance angles associated with the 7:3 mean motion commensurability between planets d and e reveals uniform circulation in each case (range ≈ 360◦), directly challenging the resonance identification of Wilson and indicating a near-resonant rather than formally resonant dynamical state. For the putative fifth body identified as an unconfirmed radial velocity signal at P ≈ 53.9 days, we derive dynamical constraints over 147,600 years (10^6 orbital periods of the candidate planet), finding that long-term stability requires $e_f \lesssim 0.12$ for most of the tested mass range (0.5–20$M_\oplus$). A pronounced instability stripe at $e_f \approx 0.296$, with mean survival times below 820 years across all tested masses, is consistent with a mean motion resonance between the candidate planet and planet e near the 11:6 commensurability. These results establish the first dedicated dynamical characterization of the LHS 1903 system and provide constraints relevant to the interpretation of its anomalous inside-out planetary architecture.

Keywords: Planetary Dynamics, Orbital Stability, N-Body Simulations, M-Dwarf Planetary Systems, Mean Motion Resonance, LHS 1903, Exoplanets, Secular Evolution, Survival Time Analysis, Compact Planetary Systems

1. Introduction

M-dwarf stars, comprising the majority of stars in the Galaxy, have emerged as some of the most productive targets in exoplanet science. Their low masses and radii amplify planetary signals relative to solar-type stars, enabling the characterization of small planets that would otherwise remain undetectable. The Transiting Exoplanet Survey Satellite has been particularly productive in this regard, discovering hundreds of planets around M-dwarfs since its launch in 2018 [4]. Compact multi-planet systems around these stars — where multiple planets orbit within a fraction of an astronomical unit — raise important questions about dynamical stability, orbital architecture, and the formation conditions that produced them.

LHS 1903 is an M-dwarf star located at 35.69 pc in the constellation Lynx, with a stellar mass of 0.538$M_\odot$, effective temperature of 3664 K, and probable thick-disk membership indicative of an old stellar population. Wilson et al. recently confirmed four transiting planets in this system using a combination of TESS photometry, Characterizing Exoplanet Satellite photometry, and HARPS-N radial velocity measurements [5]. The four planets, designated LHS 1903 b, c, d, and e, have orbital periods of 2.16, 6.23, 12.57, and 29.32 days respectively, and all reside within 0.16 AU of the host star.

The system's architecture is unusual. While the two innermost planets (b and c) bracket a pair of submeters (c and d) with

extended gaseous envelopes, the outermost planet e is a rocky super-Earth with a bulk density of $6.10^{+1.83}_{-1.71}$ g cm^{-3}, consistent with an Earth-like composition and the absence of a substantial gaseous atmosphere. This inverted arrangement — rocky, gaseous, gaseous, rocky — contradicts the standard expectation that outer planets in a protoplanetary disk should accrete more volatiles and retain thicker envelopes. Wilson et al. propose that planet e formed in a gas-depleted environment after the protoplanetary disk had been substantially cleared, offering the first strong observational case for the gas-depleted formation hypothesis.

The orbital period ratio of planets d and e (P_e/P_d = 29.32/12.57 = 2.333) is commensurate with the 7:3 mean motion resonance (MMR). Wilson et al. classify this pair as likely in resonance based on numerical orbital evolution and a possible weak transmitting variation signal. MMRs play a significant role in the long-term stability and dynamical history of compact planetary systems, acting as both stabilizing mechanisms and, when eccentricities are driven to high values, as destabilizing pathways. Whether the LHS 1903 d–e pair is formally captured in the 7:3 MMR, or merely resides near the commensurability, has direct implications for the system's dynamical history and the formation conditions of planet e [6].

Additionally, Wilson et al. identify a possible Keplerian signal at $P \approx 53.9$ days in their blind radial velocity search. If real, this would correspond to a fifth body at a semi-major axis of ≈ 0.208 AU, exterior to planet e. The authors note the signal is unconfirmed and may originate from stellar activity. Nevertheless, if confirmed, this body's dynamical influence on the known system has not been previously investigated.

No dedicated dynamical stability analysis of LHS 1903 has been published to date. In this work, we present a systematic N-body study addressing four questions:

Over what range of orbital parameters can planet e maintain long-term stability given the observed eccentricity of planet d? (2) Is stability driven primarily by mass or eccentricity? (3) Is the d–e pair formally in the 7:3 MMR? (4) What dynamical constraints apply to the putative fifth body at $P \approx 53.9$ days?

2. System Parameters

All parameters are adopted directly from Wilson et al. and the NASA Exoplanet Archive. Table 1 summarizes the values used as initial conditions in all simulations. Planetary radii are converted to AU for REBOUND's collision detection ($1R_\oplus = 4.263\times10^{-5}$ AU; $1R_\odot = 4.650 \times 10^{-3}$ AU).

3. Methods

3.1. N-body Integration

All simulations used rebound version 4.6.0 with the waist simplistic integrator and a fixed timestep $dt = 0.0003$ yr, corresponding to ≈ 5% of the orbital period of the innermost planet, LHS 1903 b (P_b = 2.16 days = 0.00591 yr). This follows the standard recommendation that a simplistic integrator's timestep should not exceed 5% of the shortest orbital period in the system to ensure adequate numerical accuracy [7].

Physical radii were assigned to all bodies including the host star (Table 1), enabling rebound's direct collision detection algorithm (microlesion = "direct"). An ejection criterion of immerit max distance = 2.0 AU was applied. A simulation is classified as unstable upon either physical collision between any two bodies or ejection of any planet beyond 2.0 AU. While the fixed timestep of waist may occasionally miss high-speed close encounters through numerical tunneling, ejection precedes physical collision in compact systems of this type, making ejection the dominant instability channel. All planets were initialized with nominal parameters from Wilson et al. including the argument of periapsis ω for each planet. The system was evolved from the center of mass frame. All planets are assumed coplanar with zero mutual inclination, consistent with the near-identical transit inclinations reported by Wilson et al. and the standard assumption for compact multi-planet systems detected via transits.

3.2. Stability Grid Construction

We constructed two-dimensional 50 × 50 parameter grids, each representing 2,500 independent five-body simulations (star + four planets). Two parameters are varied per grid; all others are held at nominal values from Table 1. We use survival time — the elapsed integration time before an instability criterion is met — as.

Parameter	Planet b	Planet c	Planet d	Planet e	Star
Mass ($M_\oplus$ / $M_\odot$)	3.28 ± 0.42	$4.55^{+0.73}_{-0.69}$	$5.96^{+1.15}_{-1.13}$	$5.79^{+1.60}_{-1.61}$	$0.538^{+0.039}_{-0.030}$
Radius ($R_\oplus$ / $R_\odot$)	1.382 ± 0.046	$2.046^{+0.078}_{-0.074}$	$2.500^{+0.078}_{-0.077}$	$1.732^{+0.059}_{-0.058}$	0.539 ± 0.014
Semi-major axis (AU)	0.02656	0.05387	0.08604	0.15135	—
Period (days)	2.1555	6.2262	12.5663	29.3177	—
Eccentricity	$0.015^{+0.014}_{-0.010}$	$0.089^{+0.036}_{-0.030}$	$0.112^{+0.055}_{-0.044}$	$0.014^{+0.015}_{-0.010}$	—
ω (deg)	216^{+80}_{-87}	288^{+38}_{-31}	233^{+29}_{-19}	263^{+63}_{-76}	—
Radius in AU (simulation)	5.89×10^{-5}	8.72×10^{-5}	1.07×10^{-4}	7.38×10^{-5}	2.506×10^{-3}

Table 1: Stellar and Planetary Parameters of LHS 1903

Note—Parameters from Wilson et al. (2026) and the NASA Exoplanet Archive. Radii in AU are used in REBOUND's direct collision detection algorithm. The stellar effective temperature is Teff = 3664 ± 70 K.

Our diagnostic, which is more informative than a binary stable/unstable classification.

Our primary grid varies m_e (1.0–12.0$M_\oplus$) against e_d (0.0–0.50). This combination is physically motivated: e_d is the largest eccentricity in the system and represents the primary perturbative threat to planet e. A secondary grid varies m_d and m_e independently (1.0– 12.0$M\oplus$ each) at nominal eccentricities to isolate the role of mass.

The primary grids were integrated for 80,000 years, equivalent to approximately 10^6 orbital periods of planet e (P_e = 0.08027 yr; 80,000/0.08027 ≈ 10^6), satisfying the standard criterion for long-term dynamical stability studies [8]. Integration proceeded in 200 chunks of 80,000/200 = 400 yr each, allowing survival time to be recorded at the moment of instability. All grids were computed in parallel using Python's multiprocessing module with 7 concurrent workers.

3.3. Putative Planet f Grid

Wilson et al. identify a possible Keplerian signal at $P \approx 53.9$ days in their blind radial velocity search. The corresponding semi-major axis, derived from Kepler's third law assuming $M_\star = 0.538M_\odot$, is $a_f \approx 0.2083$ AU. We investigate dynamical compatibility by constructing a 50 × 50 survival time grid varying m_f(0.5–20.0$M_\oplus$) against ef (0.0–0.50).

As no observational constraints on ω_f exist, we set $\omega_f = 0°$. The integration time is 147,600 years, corresponding to 10^6 orbital periods of planet f (P_f = 0.1476 yr; 147,600/0.1476 = 10^6), consistent with the standard stability criterion applied to the outermost body.

3.4. Orbital Evolution and Resonance Analysis

The nominal four-planet system was integrated for 10,000 years with one output snapshot per year. From each snapshot we extracted the semi-major axis a, eccentricity e, mean longitude $\lambda = \Omega+\omega+M$, and longitude of periapsis $\varpi = \Omega + \omega$ for all planets.

To assess the 7:3 MMR between planets d and e, we computed all five resonance angles of the form:

$$\Phi_j = 7\lambda_e - 3\lambda_d - j\,\varpi_e - (4-j)\,\varpi_d, \quad j = 0, 1, 2, 3, 4. \tag{1}$$

A resonance angle is classified as liberating if its total range remains below 180° over the integration. We additionally tracked the apsidal difference $\Delta\omega = \omega_d - \omega_e$, folded to [−180°,180°], to assess apsidal alignment as a secondary resonance signature.

4. Results

4.1. Nominal System Architecture and Orbital Evolution

Figure 1 shows the orbital architecture of LHS 1903, tracing one complete orbit of planet e (29.32 days) for all four planets. The system is compact with all planets within 0.16 AU.

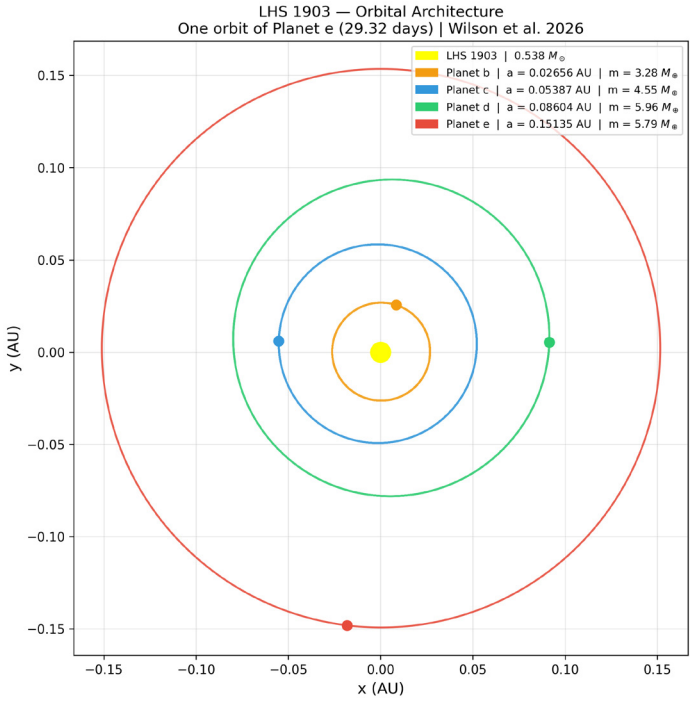

Figure 1: Orbital architecture of LHS 1903, tracing one complete orbit of planet e (29.32 days) for all four planets. The yellow circle at the centre represents the host star (0.538$M_\odot$). Coloured dots mark instantaneous planetary positions at the end of the integration. All planets are initialised with nominal orbital parameters including ω from Wilson et al.

Figure 2 shows the eccentricity evolution of all four planets over 10,000 years at nominal parameters. All planets exhibit bounded secular oscillations with no evidence of drift, confirming long-term stability. The semimajor axis variations (Figure 3) remain below 0.025% of the nominal value for every planet, confirming the orbital architecture is dynamically frozen on timescales relevant to current observational uncertainties (e.g.,Δa_e = +0.00314/ − 0.00338 AU from the NASA Exoplanet Archive).

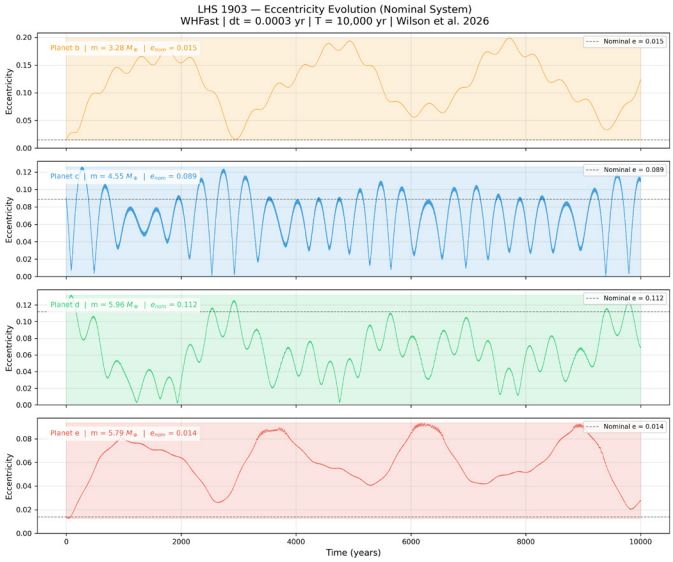

Figure 2: Eccentricity evolution of all four planets over 10,000 yr at nominal parameters. Dashed lines mark the nominal observed eccentricity. Shaded regions indicate the full oscillation envelope. Note that planet e's eccentricity varies between 0.014 and ≈ 0.085, six times its nominal value, while planet d is captured near the maximum of its secular oscillation cycle (ed ≈ 0.112). The anti-correlated oscillations of planets d and e are a signature of secular eccentricity exchange

Figure 3shows planet e's eccentricity oscillates between ≈ 0.014 and ≈ 0.085 over a secular period of ≈ 2,000 years, reaching values six times its nominal observed value. Planet d's eccentricity oscillates between ≈ 0.00 and ≈ 0.12, with the nominal value of 0.112 captured near the maximum of its secular cycle. The two oscillations are anticorrelated, a signature of secular eccentricity exchange between gravitationally coupled planets.

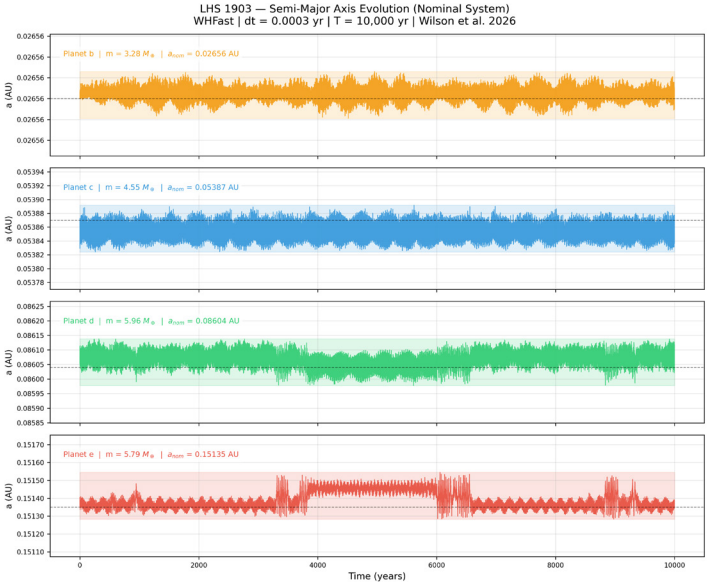

Figure 3: Semi-major axis evolution of all four planets over 10,000 yr. Dashed lines mark the nominal semi-major axis from Wilson et al. All panels show variations below 0.025% of the nominal value, confirming the orbital architecture is dynamically frozen on timescales relevant to current observational uncertainties

Figure 4 shows the phase space trajectory of the d– e eccentricity pair over 10,000 years, with one point per year encoded in time using the plasma colourmap. The trajectory is confined to e_d ∈ [0.00,0.13] and e_e ∈ [0.01,0.09], forming a bounded quasi-periodic Lissajous type structure that constitutes direct visual confirmation of long-term stability. The complex topology reflects the superposition of a fast ≈ 400 yr secular mode driven by planet c and a slower ≈ 2,000 yr mode from direct d–e coupling.

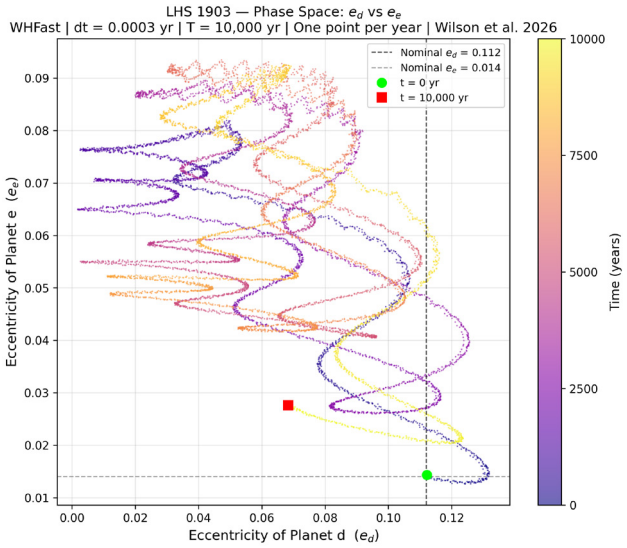

Figure 4: Phase space trajectory of the d–e eccentricity pair over 10,000 yr, with one point per year. The plasma colourmap encodes time from dark purple (t = 0) to bright yellow (t = 10,000 yr). Green circle: initial position at nominal values. Red square: final position at t = 10,000 yr. The bounded quasi-periodic Lissajous structure confirms long-term dynamical stability. The complex topology reflects superposition of a fast ≈ 400 yr secular mode from planet c and a slower ≈ 2,000 yr mode from direct d–e coupling

4.2. Stability Coastline: me versus e_d

Figure 5 shows the primary result: a 50 × 50 survival time map varying m_e (1.0–12.0$M_\oplus$) against e_d (0.0– 0.50) integrated for 80,000 years. Of 2,500 simulations, 1,435 (57.4%) survived the full integration and 1,065 (42.6%) destabilized. The mean survival time among unstable configurations was 9,868 yr.

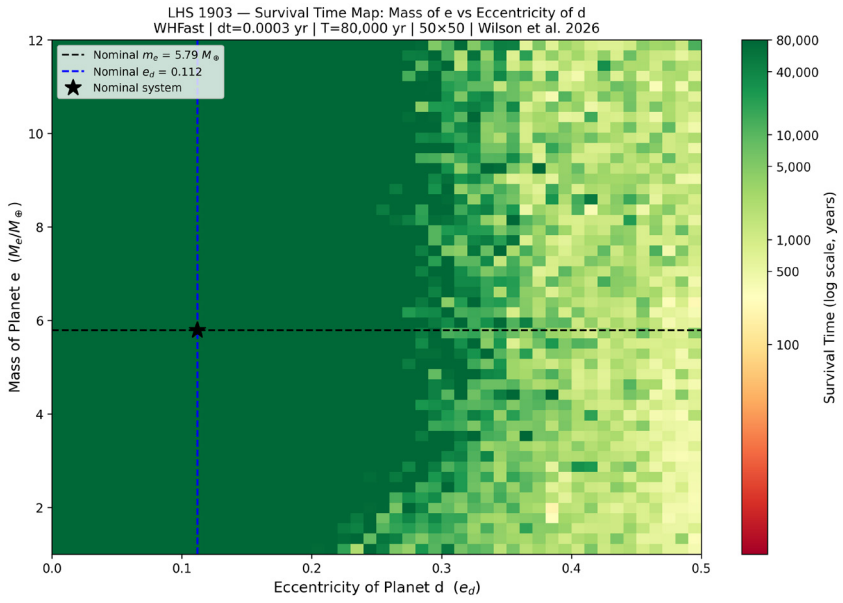

Figure 5: Survival time map for me vs ed, integrated for 80,000 yr on a 50 × 50 grid. Colour encodes survival time on a logarithmic scale from red (short-lived) to dark green (full integration survived). Dashed lines mark nominal parameter values; the star symbol marks the nominal system. Of 2,500 simulations, 1,435 (57.4%) survived the full integration. The stability coastline runs diagonally from e_d ≈ 0.214 at me = 1$M_\oplus$ to a peak of e_d ≈ 0.388 near me ≈ 4.4$M_\oplus$, giving a stability margin Δe_d ≈ 0.184 at the nominal mass

The nominal system position (star symbol at e_d = 0.112, m_e = 5.79$M_\oplus$) survives the full 80,000 yr integration. At the nominal mass, the stability boundary lies at $e_d \approx 0.296$, giving a stability margin $\Delta e_d \approx 0.184$: planet d's eccentricity would need to increase by a factor of ≈ 2.6 from its observed value to destabilize the system.

The stability coastline runs diagonally with a weak, non-monotonic mass dependence. At $m_e = 1.0M_\oplus$ the maximum stable eccentricity is e_d = 0.214; this rises to $e_d \approx 0.388$ near $m_e \approx 4.4M_\oplus$ before declining to $e_d \approx 0.276$ at $m_e = 12.0M_\oplus$. The minimum survival time across the grid is 199 yr, occurring at high eccentricity configurations remote from the nominal system. The transition zone between the stable and unstable regions spans $\Delta e_d \approx 0.10$–0.15 in eccentricity width, reflecting gradual onset of instability rather than a sharp bifurcation.

4.3. Mass of Planet e versus Mass of Planet d

Figure 6 shows the 50×50 survival time map varying m_d and m_e independently (1.0–12.0$M_\oplus$ each) at nominal eccentricities, integrated for 80,000 years. All 400 simulations (N_{grid} = 20 × 20) survived the full integration. This result directly demonstrates that planetary mass is not a driver of instability at observed eccentricities: even doubling or tripling the masses of planets d and e from their measured values does not destabilize the system. Eccentricity, not mass, is the dominant stability parameter.

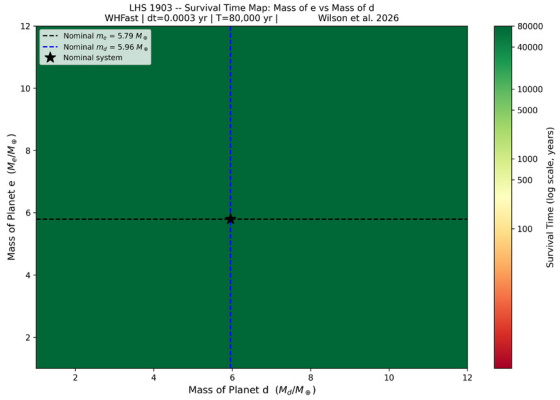

Figure 6: Survival time map for me vs md at nominal eccentricities, integrated for 80,000 yr on a 20×20 grid. The uniformly dark green map (100% stability across all 400 simulations) confirms that mass variations alone cannot drive instability at observed eccentricities, establishing ed as the dominant stability parameter

4.4. The 7:3 Mean Motion Commensurability

Figure 7 shows the apsidal resonance analysis for planets d and e. Both ω_d and ω_e circulate independently, with differing precession rates confirming the absence of apsidal locking. The apsidal difference $\Delta\omega$ circulates through the full ±180◦ range with a period of ≈ 1,000– 1,500 yr.

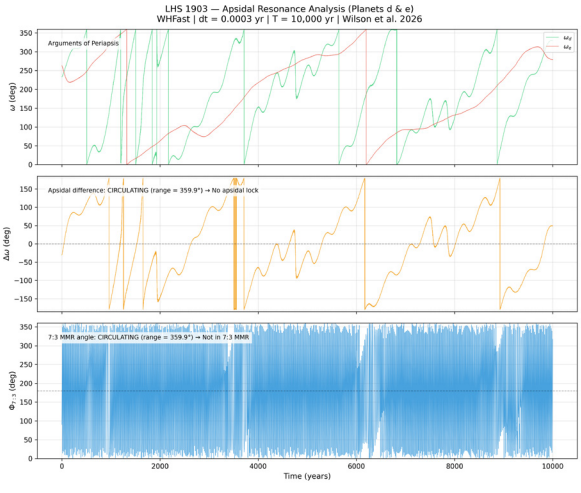

Figure 7: Apsidal resonance analysis for planets d and e over 10,000 yr. Top: arguments of periapsis ωd (green) and ωe (red); vertical discontinuities are the 0◦/360◦ wrapping. Middle: apsidal difference Δω = ωd − ωe folded to [−180◦, 180◦]; circulation through the full range confirms no apsidal locking. Bottom: primary 7:3 resonance angle Φ1 = 7λe − 3λd − 4ϖe, circulating through 360◦

Figure 8 shows all five resonance angles Φ_j (Equation 1) computed simultaneously over 10,000 years. Every angle spans the full 0◦–360◦ range with a measured range of 359.9◦ in each case, indicating uniform circulation with no preferential liberation center. This is the defining signature of a system not formally captured in the 7:3 MMR.

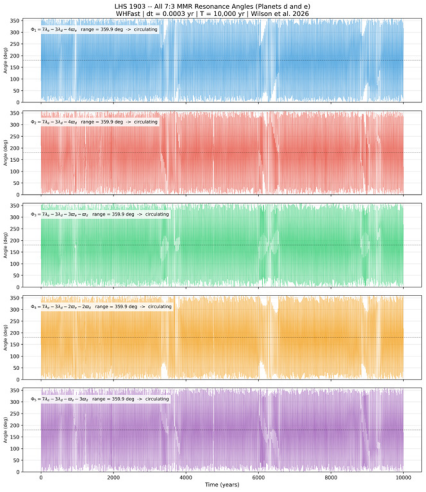

Figure 8: All five 7:3 MMR resonance angles Φj (Equation 1) for j = 0, 1, 2, 3, 4 over 10,000 yr. Every angle spans ≈ 360◦ (measured range = 359.9◦ in each case), confirming the d–e pair is not formally captured in the 7:3 MMR at the nominal orbital configuration

This result is in tension with the resonance identification of Wilson et al., who classify the d–e pair as "likely" in the 7:3 MMR based on their numerical orbital evolution analysis. We note that $P_e/P_d = 2.333$ satisfies the necessary but not sufficient condition for resonance capture, which additionally requires appropriate eccentricities and orbital phases to sustain liberation of at least one resonance angle [9]. The circulating behavior observed here across all five angles, with initial conditions drawn directly from Wilson et al., indicates the system presently occupies a near resonant but non-resonant dynamical state. We suggest that the low eccentricity of planet e ($e_e = 0.014$) may be insufficient to sustain resonant liberation in this commensurability.

4.5. Dynamical Constraints on Putative Planet f

Figure 9 shows the 50 × 50 survival time map for putative planet f, varying m_f (0.5–20.0$M_\oplus$) against e_f (0.0–0.50), integrated for 147,600 years. Of 2,500 simulations, 710 (28.4%) survived the full integration and 1,790 (71.6%) destabilized. The minimum survival time is 0.3 yr.

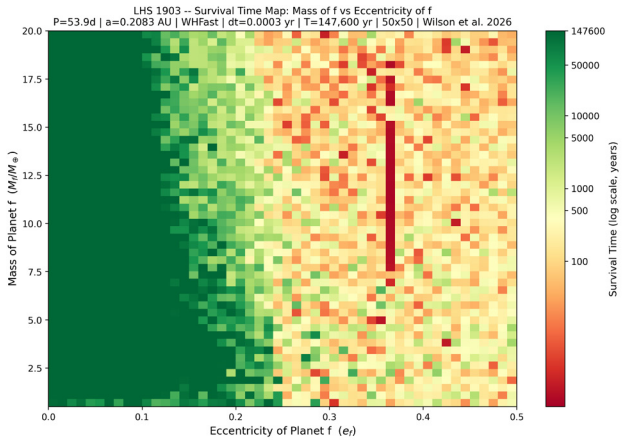

Figure 9: Survival time map for putative planet f, varying mf (0.5–20.0M⊕) against ef (0.0–0.50), integrated for 147,600 yr on a 50 × 50 grid. Of 2,500 simulations, 710 (28.4%) survived the full integration. The stability boundary at ef ≈ 0.12 (below which 98.2% of simulations survive) is clearly defined. The dark-red instability stripe at ef ≈ 0.296 spans all tested masses with mean survival times < 820 yr, consistent with the 11:6 MMR between planet f and planet e

The stability boundary lies at $e_f \approx 0.12$, below which 98.2% of simulations survive the full integration regardless of mass. This threshold shows a weak mass dependence: at low masses ($m_f \approx 0.5 M_\oplus$) the boundary extends to $e_f \approx 0.235$, tightening to $e_f \approx 0.092$ at $m_f \approx 18$–$20 M_\oplus$. At the reference mass $m_f = 5.79 M_\oplus$, the maximum stable eccentricity is ef = 0.184.

The most striking feature is a narrow vertical instability stripe at $e_f \approx 0.296$, spanning the full mass range with mean survival times of 819 yr at $e_f = 0.296$ and 524 yr at $e_f = 0.306$. This feature is consistent with a MMR between planet f and planet e near the 11:6 commensurability ($P_f/P_e = 53.9/29.32 = 1.838 \approx 11/6 = 1.833$). At this eccentricity, the apocentre of planet f's orbit approaches the orbit of planet e, triggering rapid resonant destabilization independent of mass.

Configurations with $e_f > 0.35$ are uniformly short-lived across all tested masses. These results establish clear dynamical upper limits on the orbital eccentricity of any fifth body at $P \approx 53.9$ days.

4.6. Eccentricity of Planet d versus Eccentricity of Planet e

Figure 10 shows the 50 × 50 survival time map varying e_d (0.0–0.50) against e_e (0.0–0.30), integrated for 80,000 years. Of 2,500 simulations, 1,062 (42.5%) survived the full integration and 1,438 (57.5%) destabilized. The mean survival time among unstable configurations was 11,519 yr.

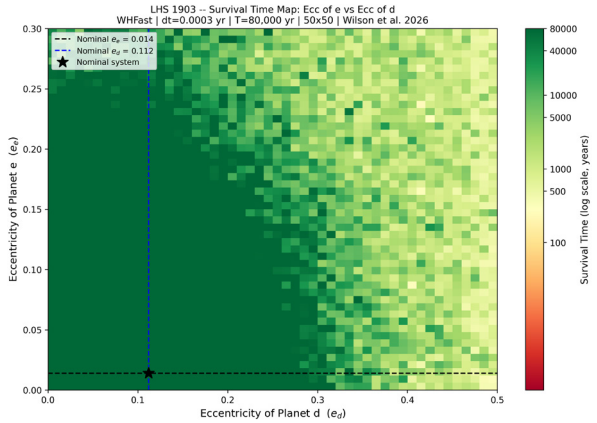

Figure 10: Survival time map for ee vs ed, integrated for 80,000 yr on a 50 × 50 grid. Of 2,500 simulations, 1,062 (42.5%) survived the full integration. The stability coastline is not vertical: the maximum stable ed decreases systematically from ≈ 0.316 at ee = 0.0 to ≈ 0.112 at ee = 0.276, demonstrating that planet e's eccentricity is a secondary but non-negligible stability parameter. The nominal system (star symbol) survives the full integration

The nominal system (star symbol at $e_d = 0.112$, $e_e = 0.014$) survives the full integration. The stability coastline is not vertical as might be expected if ee were entirely irrelevant. Instead, the maximum stable ed decreases systematically with increasing e_e: from $e_d \approx 0.316$ at $e_e = 0.0$ to $e_d \approx 0.245$ at $e_e = 0.153$ and $e_d \approx 0.112$ at $e_e = 0.276$. The total variation in the coastline across the tested range of e_e is $\Delta e_d \approx 0.235$, comparable in magnitude to the coastline variation with me found in Section 4.2.

This result is physically meaningful: a higher eccentricity of planet e places it on a more elongated orbit that periodically brings it closer to planet d's orbit, reducing the effective dynamical separation and lowering the eccentricity threshold at which destabilization occurs. While e_e is currently very low (0.014), our eccentricity evolution analysis (Section 4.1) shows that ee naturally reaches ≈ 0.085 during the secular cycle. From Figure 10, at $e_e = 0.085$ the maximum stable ed is approximately 0.28, which remains comfortably above the observed $e_d = 0.112$ but is measurably lower than the boundary at $e_e \approx 0$. The stability of the system therefore depends on the secular average of ee rather than just its instantaneous observed value.

5. Discussion

5.1. Stability and the Observed Eccentricity of Planet d

The stability margin $\Delta e_d \approx 0.184$ indicates LHS 1903 is dynamically comfortable rather than marginal at its observed configuration. This is significant because $e_d = 0.112$ is itself near the maximum of planet d's secular eccentricity cycle: had the measurement been obtained near secular minimum ($e_d \approx 0.00$–0.03), the apparent margin would appear even larger. The system is therefore stable not only at the observed snapshot but across the full secular oscillation.

The non-monotonic mass dependence of the coastline — with a stability peak near $m_e \approx 4$–$5 M_\oplus$ — is consistent with mass-dependent proximity to secondary resonances within the parameter space. The possibility that specific mass ratios within the tested range fall near additional commensurabilities warrants investigation with finer mass resolution in future work.

5.2. The Near-Resonant Configuration

The circulation of all five 7:3 MMR resonance angles challenges the resonance identification of Wilson et al., but this does not render the near commensurability physically irrelevant.

Near-resonant systems are known to exhibit enhanced secular eccentricity exchange relative to purely secular systems, and the large-amplitude eccentricity oscillations we observe for both planets d and e may be partly driven by proximity to the 7:3 resonance even without formal capture. The near-zero eccentricity episodes for planet d at the trough of its secular cycle, reaching $e_d \approx 0.00$, are particularly striking and may reflect this near-resonant amplification.

We caution that our result is based on integration of the nominal orbital configuration. Given the substantial observational uncertainties on e_d (+0.055/−0.044) and e_e (+0.015/−0.010), orbital configurations within the 1σ error bars could in principle produce different resonance angle behavior. A Monte Carlo analysis sampling from the full posterior distributions of the orbital parameters would be required to make a definitive statement, and is beyond the scope of this work. We therefore interpret our result as strongly challenging but not definitively overturning the resonance hypothesis of Wilson et al.

5.3. Implications for Planet f

The eccentricity constraint $e_f \lesssim 0.12$ for the putative planet at $P \approx 53.9$ days is stringent. If the signal is of planetary origin, the body would need to occupy a near-circular orbit — a configuration more consistent with formation in a dynamically cold disk than with significant post-formation scattering. Conversely, if future RV observations confirm planet f with $e_f \approx 0.30$, the extreme instability we find at this eccentricity (survival times < 820 yr) would represent a strong argument against the planetary interpretation of the 53.9-day signal, pointing instead to stellar activity as the origin. The instability stripe at $e_f \approx 0.296$ associated with the putative 11:6 resonance with planet e may therefore serve as a useful discriminator between planetary and activity driven interpretations once the signal is better characterized.

We also note that Wilson et al., specifically flag the proximity of the 53.9-day period to harmonics of the stellar rotation period (40.8 days) as a concern for the planetary interpretation. Our dynamical analysis is independent of and complementary to this spectroscopic argument.

5.4. Limitations

Several limitations of this study should be noted.

• **Coplanarit:** We have assumed zero mutual inclination throughout. Mutual inclinations, if present, can alter resonance angles and stability boundaries. Long baseline radial velocity monitoring or precise transit timing variation measurements would be required to constrain inclinations for this system.

• **General Relativistic Precession:** GR precession has not been included in our simulations. The GR apsidal precession rate for each planet is given by

$$\dot{\omega}_{\rm GR} = \frac{3GM_\star n}{a\,c^2(1-e^2)}, \tag{2}$$

where $n = 2\pi/P$ is the mean motion. For LHS 1903, the calculated rates are: planet b: 0.0366 deg yr^{-1} (365.6◦ per 10,000 yr); planet c: 0.0063 deg yr^{-1} (62.9◦ per 10,000 yr); planet d: 0.0020 deg yr^{-1} (19.6◦ per 10,000 yr); planet e: 0.0005 deg yr^{-1} (4.7◦ per 10,000 yr). The GR precession of planet b is substantial — ≈ 366◦ per 10,000 yr — and may affect the secular interactions between the inner planets on the timescales we have studied. For planets d and e, the GR precession rates are more modest (19.6◦ and 4.7◦ per 10,000 yr respectively), but the cumulative effect over 80,000 yr (156.8◦ and 37.7◦) could influence the resonance angle behaviour reported in Section 4.4. GR precession tends to suppress resonance capture by advancing inner-planet apsidal precession rates away from resonant values; its inclusion in future work may further support our finding that the d–e pair is not formally in the 7:3 MMR.

• ***Integration Timescale:*** While our survival time maps satisfy the 106-orbit criterion, they do not exclude very slow chaotic diffusion on timescales of 107–108 years. Long-term stability on Gyr timescales would require substantially longer integrations or analytical secular theory.

• ***MEGNO Chaos Indicator:*** We attempted to compute MEGNO chaos indicators using both waist and ias15 [10,11]. The fast-orbital period of planet b (2.16 days) caused the variational equations required for MEGNO to produce unreliable results regardless of integrator or timestep choice, a known limitation for compact systems with large period ratios between inner and outer planets. We therefore relied solely on survival time analysis.

6. Conclusion

We have presented the first dedicated dynamical stability analysis of the LHS 1903 exoplanetary system. Our principal conclusions are:

• *The nominal system is robustly stable.* The nominal configuration survives 80,000 yr of integration, with a stability margin $\Delta e_d \approx 0.184$ at the observed mass of planet e. Planet d's eccentricity would need to increase by a factor of ≈ 2.6 to destabilize the system [12].

• *Eccentricity of planet d is the dominant stability parameter, but ee is not irrelevant.* A 50 × 50 survival time map varying m_d and m_e independently at nominal eccentricities produces 100% stability, confirming mass alone cannot drive instability. However, the e_d vs e_e survival time map reveals that the stability coastline decreases systematically with increasing e_e, from $e_d \approx 0.316$ at $e_e = 0.0$ to $e_d \approx 0.112$ at ee = 0.276. Planet e's secular eccentricity excursions to ee ≈ 0.085 therefore modestly tighten the effective stability boundary on secular timescales.

• *The d–e pair is not formally in the 7:3 MMR.* All five resonance angles of the 7:3 commensurability circulate through ≈ 360◦, directly challenging Wilson et al. (2026). The d–e pair occupies a near-resonant but non-resonant dynamical state. The large-amplitude secular eccentricity oscillations may nevertheless be

partially driven by proximity to the commensurability.

• *Putative planet f is constrained to* $e_f \lesssim 0.12$. A 50 × 50 survival time map over 147,600 yr establishes this eccentricity threshold for most tested masses. A pronounced instability stripe at $e_f \approx 0.296$, consistent with the 11:6 commensurability with planet e, produces mean survival times below 820 yr across all tested masses and may serve as a discriminator between planetary and stellar activity interpretations of the 53.9-day RV signal.

These results provide the first quantitative dynamical characterization of the LHS 1903 system, establish observational constraints on the candidate fifth body, and motivate further study of the system's secular architecture with general relativistic corrections and Monte Carlo orbital sampling.

• This research made use of the rebound N-body integration package. 3 Orbital and stellar parameters were obtained from the 4 NASA Exoplanet Archive, which is operated by the California Institute of Technology, under contract with the 6 National Aeronautics and Space Administration under 7 the Exoplanet Exploration Program.

• ***Facilities:*** TESS, CHEOPS, HARPS-N, NASA Ex-oplanet Archive.

• ***Software:*** Rebound [13].

References

1. Wilson, T. G. (2026). Gas-depleted planet formation occurred in the four-planet system around the red dwarf LHS 1903. Science, eadl2348.
2. Rein, H., & Liu, S. F. (2012). REBOUND: an open-source multi-purpose N-body code for collisional dynamics. Astronomy & Astrophysics, 537, A128.
3. Rein, H., & Tamayo, D. (2015). WHFAST: a fast and unbiased implementation of a symplectic Wisdom–Holman integrator for long-term gravitational simulations. Monthly Notices of the Royal Astronomical Society, 452(1), 376-388.
4. Ricker, G. R., Winn, J. N., Vanderspek, R., Latham, D. W., Bakos, G. Á., Bean, J. L., ... & Villasenor, J. (2015). Transiting exoplanet survey satellite. Journal of Astronomical Telescopes, Instruments, and Systems, 1(1), 014003-014003.
5. Benz, W., Broeg, C., Fortier, A., Rando, N., Beck, T., Beck, M., .& Wolter, D. (2021). The CHEOPS mission. Experimental Astronomy, 51(1), 109-151.
6. Lithwick, Y., & Wu, Y. (2012). Resonant repulsion of Kepler planet pairs. The Astrophysical Journal Letters, 756(1), L11.
7. Wisdom, J., & Holman, M. (1991). Symplectic maps for the n-body problem. Astronomical Journal (ISSN 0004-6256), vol. 102, Oct. 1991, p. 1528-1538., 102, 1528-1538.
8. Gladman, B. (1993). Dynamics of systems of two close planets. Icarus, 106(1), 247-263.
9. Murray, C. D., & Dermott, S. F. (1999). Solar system dynamics. Cambridge university press.
10. Cincotta, P. M., & Simó, C. (2000). Simple tools to study global dynamics in non-axisymmetric galactic potentials–I. Astronomy and Astrophysics Supplement Series, 147(2), 205-228.
11. Rein, H., & Spiegel, D. S. (2015). IAS15: a fast, adaptive, high-order integrator for gravitational dynamics, accurate to machine precision over a billion orbits. Monthly Notices of the Royal Astronomical Society, 446(2), 1424-1437.
12. Harris, C. R. (2020). Array programming with NumPy. Nature. 585, 357.
13. Hunter, J. D. (2007). Matplotlib: A 2D graphics environment. Computing in science & engineering, 9(3),90-95.